Preparation and Characterization of $Ag@TiO_2$ Core-Shell Nanoparticles in Water-in-Oil Emulsions

Dan Zhang,[a] Ximing Song,[b] Rongwei Zhang,[a] Ming Zhang,[a] and Fengqi Liu*[a]

Keywords: Silver / Titanium / Core-shell nanoparticles / Water-in-oil emulsion / Surface photovoltaic spectroscopy

We report a simple route for the effective synthesis of $Ag@TiO_2$ nanoparticles in water-in-oil (w/o) emulsions and provide detailed characterization of the materials with TEM, TG-DTA, IR, XRD, and SPS measurements. Such core-shell hybrid nanoparticles can be fabricated in two simple steps: the formation of the silver core by the reduction of a Tollens reagent with glucose in the water phase, and the hydrolysis of $Ti(OC_4H_9)_4$ at the water/oil interface for the formation of the amorphous TiO_2 shell. The procedure led to the formation of nanocomposites with a crystalline core in a size range from 5 to 15 nm in diameter and an amorphous shell of 6–10 nm thickness in a typical synthesis. The shell was converted to crystalline oxide upon thermal treatment. Surface photovoltaic spectroscopy (SPS) measurements indicate that the materials have potential for application in photoinduced electron storage and photocatalysis.
(© Wiley-VCH Verlag GmbH & Co. KGaA, 69451 Weinheim, Germany, 2005)

Introduction

Core-shell metal nanoparticles with oxide shells have attracted considerable attention owing to their stability under extreme conditions,[1] and their optical and catalytic properties.[2–3] The shells offer protection to the cores as well as introducing new properties to the hybrid structures.[4] An important shell-forming material is TiO_2, which offers wide-ranging properties.[5] A number of methods have been used to prepare the core-shell metal nanoparticles.[1,6–8] Among these methods are citrate reduction,[9] borohydride reduction,[10] sonochemical methods,[11] radiolytic reduction,[12] and metal evaporation-condensation.[13] It was shown that the size, composition, and structure of the resultant particles depended on the preparation conditions.

Water-in-oil (w/o) emulsions are thermodynamically stable with nanosized water droplets that are dispersed in a continuous oil phase and stabilized by surfactant molecules at the water/oil interface. The surfactant-stabilized water pools provide a microenvironment for the preparation of nanoparticles by preventing the excessive aggregation of particles. As a result, the particles obtained in such a medium are generally very fine and monodisperse. Many kinds of nanoparticles have been prepared in w/o emulsions including metals,[14] metal oxides,[15] and organic polymers.[16] However, within the limits of our knowledge, the preparation of core-shell metal nanoparticles with oxide shells in w/o emulsions has not been reported yet. In this paper, we describe an effective method for the preparation of $Ag@TiO_2$ nanoparticles in w/o emulsions and provide detailed characterization of the materials. We shall also touch upon one property we are pursuing currently, namely, surface photovoltaic spectroscopy.

[a] College of Chemistry, Jilin University,
Changchun, 130023, People's Republic of China
Fax: +86-431-8499158
E-mail: fengqiliu@21cn.com
[b] School of Chemical Science and Engineering, Liaoning University
Shenyang, 110036, People's Republic of China
Fax: +86-24-62202380
E-mail: xmsong@lnu.edu.cn
Supporting information for this article is available on the WWW under http://www.eurjic.org or from the author.

Results and Discussion

$Ag@TiO_2$ nanoparticles were fabricated in two simple steps: the formation of the silver core by the reduction of a Tollens reagent with glucose in the water phase of the water-in-oil emulsions, and the hydrolysis of $Ti(OC_4H_9)_4$ (TOB) at the water/oil interface for the formation of the amorphous TiO_2 shell. The water and organic impurities in the as-obtained emulsions containing $Ag@TiO_2$ nanoparticles were removed by vacuum-drying followed by calcination. 0.559 g of $Ag@TiO_2$ nanoparticles were obtained after calcination at 800 °C for 4 h in a typical preparation, and the product yield was approximately 100%.

The transmission electron microscopy (TEM) images and the electron diffraction diagram in Figure 1 clearly illustrate the core-shell structure of $Ag@TiO_2$ nanoparticles with a crystalline core of size 5–15 nm and an amorphous shell of thickness 6–10 nm. The size of the nanoparticles is moderately uniform. There appears some nonuniformity in the shell thickness, but the coverage is complete. In Figure 1 (see B), no diffraction is seen from the amorphous shells at room temperature, but the core manifests bulk fcc patterns. (111), (200), (220), and (311) zone axes are observed.[17]

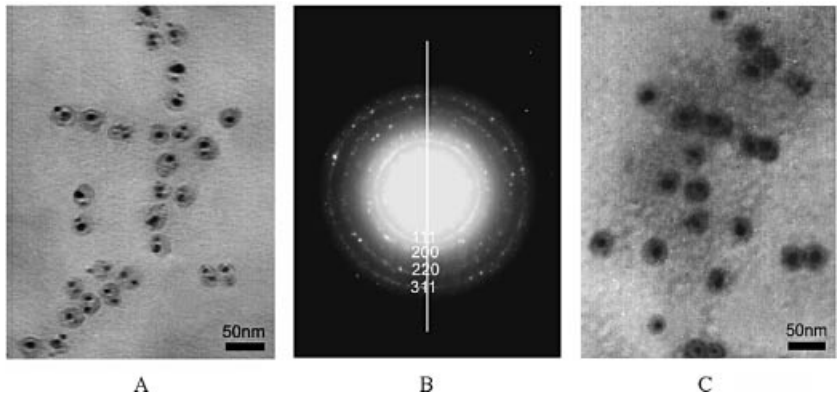

Figure 1. Transmission electron micrographs (A, C) and electron diffraction pattern (B) of $Ag@TiO_2$ nanoparticles. (A) Nanocomposites prepared from 0.59 mmol Ag^+ and 5.9 mmol TOB (wt.-% of Ag: 11.9). (C) Nanocomposites prepared from 0.59 mmol Ag^+ and 7.0 mmol TOB (wt.-% of Ag: 10.2).

The wt.-% of the core component has an influence on the properties of core-shell nanoparticles. In this work, the wt.-% of the Ag component in the nanocomposites could be adjusted by changing the molar ratio of TOB to Ag^+ in the Tollens reagent. From Figure 1 (see A and C), we can conclude that the size of the Ag core does not change and the shell thickness increases with increasing TOB at a fixed amount of Ag^+ in the Tollens reagent, i.e. with the decrease of the relative amount of Ag in the nanocomposites. The variation of the amount of Ag can lead to the formation of nanocomposites with various morphologies. The single-core nanocomposites with various shell thicknesses are the major morphology when the wt.-% of Ag is less than 11.9%, and the multicore nanocomposites are formed when the wt.-% of Ag equals 35.7%, as shown in Figure S2 in the Supporting Information.

The thermal analysis (TG-DTA) curves are shown in Figure 2. The TG curve could be divided into three main stages during the weight loss process of the $Ag@TiO_2$ sample. The first stage was in the range of 100–200 °C, corresponding to desorption or release of solvent and water in the sample. The second stage occurred in the range of 200–500 °C, which resulted mainly from the combustion and decomposition of organic matter, for example Span80, Op10, and butanol, produced from the hydrolysis of TOB. The third loss, less than 4%, was not very obvious in the range 500–700 °C, and was attributed to the dissociation of hydroxyl groups from the surface of TiO_2 nanoparticles. Hydroxyl groups were present in the infrared spectra until the samples were heated to 500 °C. It is well known that there are two types of surface OH groups, terminal Ti–OH and bridge Ti–(OH)–Ti. The dissociation temperatures of these

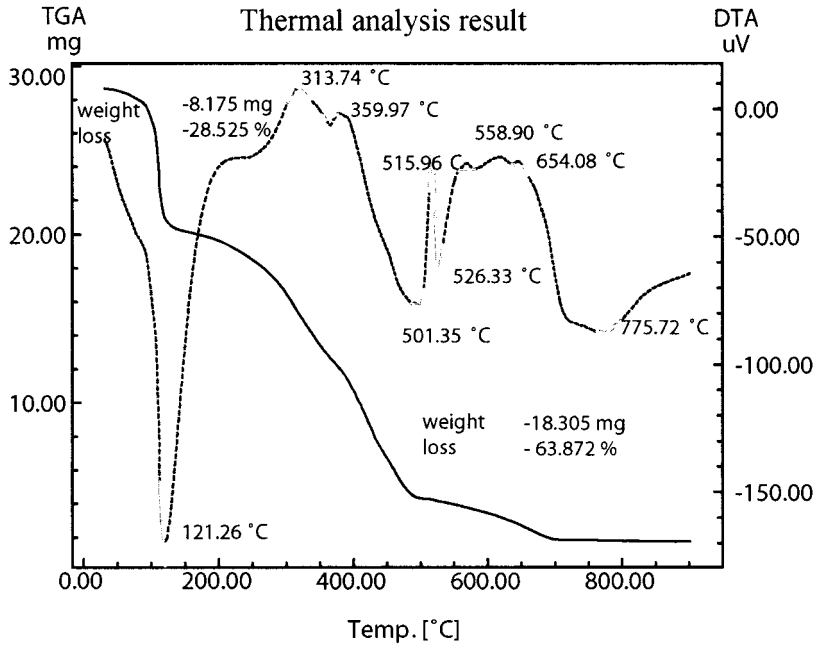

Figure 2. TG-DTA curves of $Ag@TiO_2$ nanoparticles in a typical synthesis.

 © 2005 Wiley-VCH Verlag GmbH & Co. KGaA, Weinheim

surface OH groups differ from each other, and each temperature could also be affected by the chemical surroundings. Thus the decrease in weight appears over a wide temperature range.[18] The DTA curve exhibits a decalescence peak at 121 °C, which corresponds to the desorption or release of solvent and water in the sample . Furthermore, two releasing thermal peaks can be observed at 314 and 360 °C, both corresponding to the combustion and decomposition of the organic matter, and some decalescence and releasing thermal peaks over the range 500–800 °C are also present; they result from the phase transition of TiO_2 from amorphous to anatase (around 500 °C), the dissociation of surface hydroxyl groups (500–700 °C) and the phase transition of TiO_2 from anatase to rutile (around 775 °C). As the oxide cover is solvated with unclear stoichiometry, we did not attempt to analyze the data further.

X-ray powder diffraction (XRD) analysis is usually used for the identification of core-shell structures and crystal phase as well as the estimation of crystallite size.[18] The XRD patterns of TiO_2 and Ag@TiO_2 nanoparticles calcined at 300–800 °C are shown in Figure 3. The peaks at 38°, 44°, 64°, 77° in Figure 3 (see B) are due to the (111), (200), (220), and (311) reflections of the Ag core.[1] Upon thermal treatment to 500 °C for 4 h, an obvious pattern resembling a mixture of anatase and Ag appears (note the peak at 25.3°[19]). The peaks remained almost the same even when the sample was calcined at 700 °C. However, an obvious pattern resembling a mixture of rutile and Ag appeared after calcination at 800 °C for 4 h (note the peak at 27.9°[20]). The phase transformations of the TiO_2 shell from amorphous to anatase and from anatase to rutile occurred with the increase of the calcination temperature, which was in good agreement with the results of TG-DTA. The phase transformation of TiO_2 from anatase, a crystal phase with catalytic activity, to rutile usually occurs at 500–600 °C.[18] However, in our experiments, both TiO_2 and Ag@TiO_2 nanoparticles prepared in the same system of inverse emulsion kept their anatase structure after calcination at 700 °C for 4 h (Figure 3). This observation opens up new possibilities for the application of photocatalysis over a wider temperature range. The effect of preparation methods on the phase-transformation temperature of TiO_2 from anatase to rutile needs further investigation.

The surface photovoltaic spectroscopy (SPS) technique provides a rapid, nondestructive monitor of the surface or interface properties of semiconductors such as TiO_2 and ZnO.[21] The particle size and the surface or interface properties of semiconductors are two important factors affecting the SPS response by influencing the separation efficiency of photoinduced electron–hole pairs.[22] Compared with the bulk or large particles of a semiconductor, the mechanism of SPS generation in a nanosized semiconductor is quite different, and causes the weak SPS signal of a semiconductor nanoparticle.[23] It was found that the smaller the size the weaker the SPS signal of TiO_2 or ZnO nanoparticles.[24] Moreover, the SPS signal of ZnO nanoparticles becomes much weaker when an appropriate amount of nanosized noble metal (Ag or Pd) is deposited on their surface. This

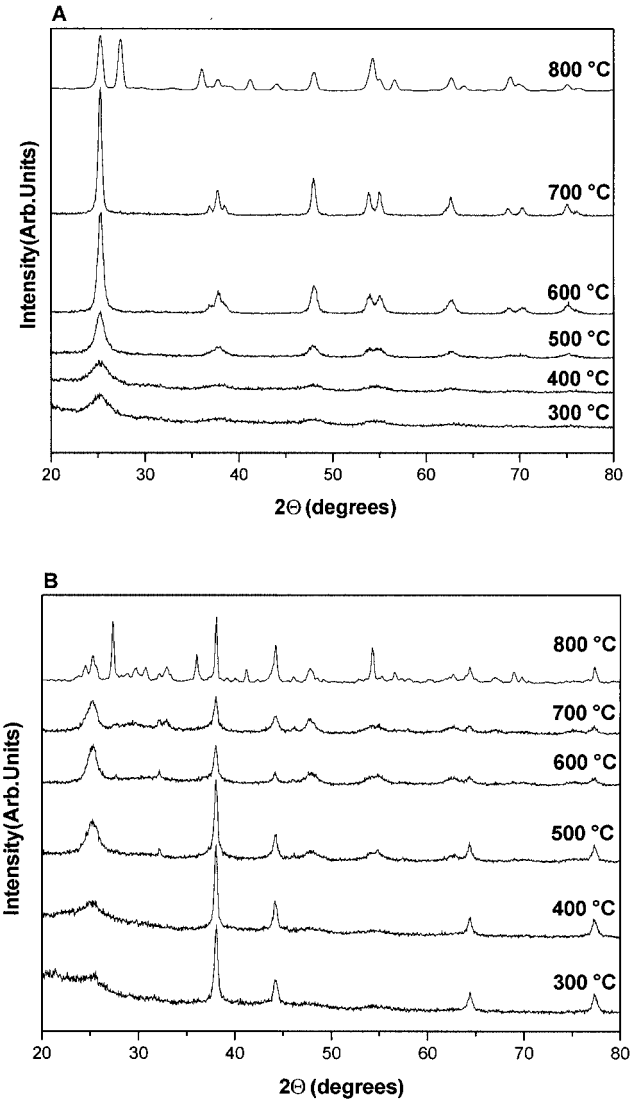

Figure 3. XRD patterns of TiO_2 (A) and Ag@TiO_2 (B) nanoparticles with 11.9% (wt.-%) Ag in a typical synthesis calcined at various temperatures.

may result from the fact that noble metal clusters effectively trap photoinduced electrons.[22]

SPS responses of Ag@TiO_2 and TiO_2 nanoparticles prepared in the same system of inverse emulsion after calcination from 500 °C to 800 °C are shown in Figure 4. The SPS response peaks at 300–400 nm can be attributed to the electron transition from the valence band to the conduction band of TiO_2 ($O_{2p}\rightarrow Ti_{3d}$).[22] The thresholds and surface photovoltages (SPV) obtained from Figure 4 as well as the sizes of the nanoparticles are summarized in Table 1. The red shift of SPS response peaks and the blue shift of thresholds with the increase of calcination temperature may be caused by the quantum size effect.[23] The threshold of Ag@TiO_2 is higher than that of TiO_2 at each calcination temperature (see Table 1) because the Ag core traps photoinduced electrons. The increase in the threshold after the formation of the core-shell structure results in the broadening

 © 2005 Wiley-VCH Verlag GmbH & Co. KGaA, Weinheim

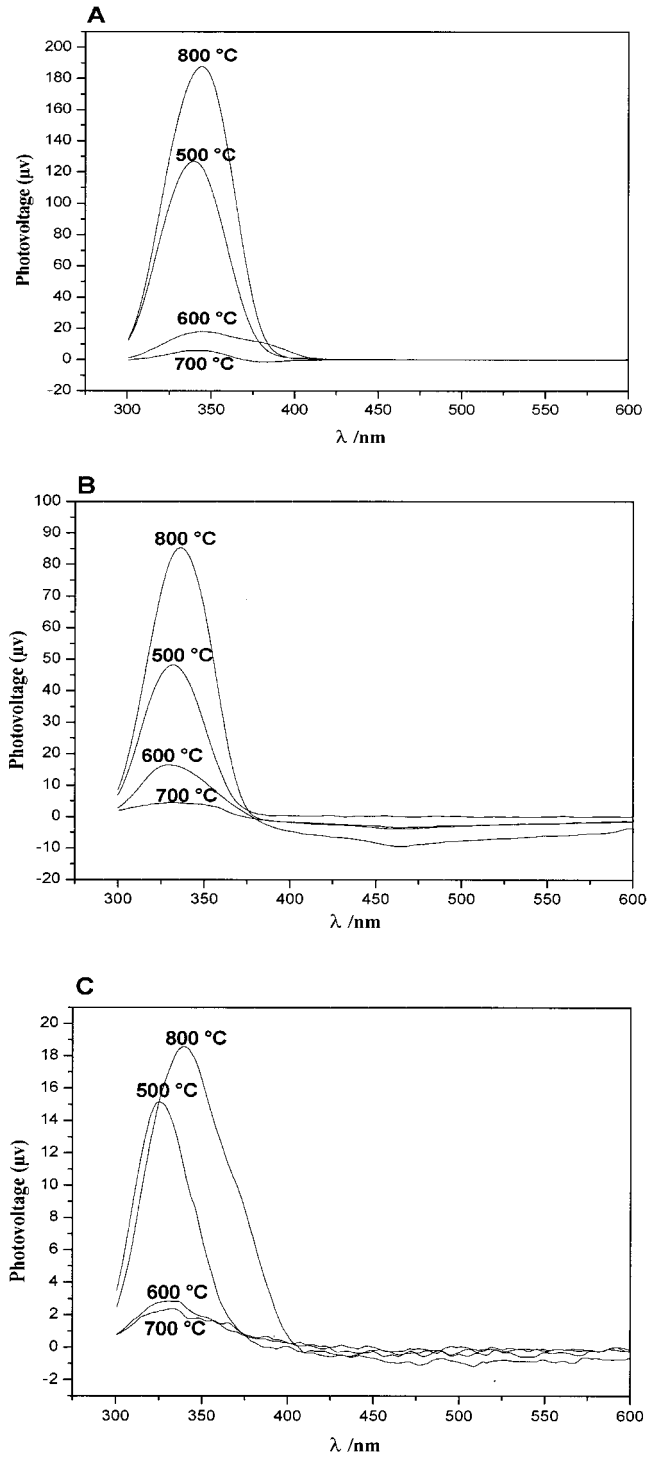

Figure 4. SPS responses of TiO_2 (A) and $Ag@TiO_2$ (B and C) nanoparticles calcined at various temperatures. (B) Nanocomposites prepared from 0.59 mmol Ag^+ and 7.0 mmol TOB (wt.-% of Ag: 10.2). (C) Nanocomposites prepared from 0.59 mmol Ag^+ and 5.9 mmol TOB (wt.-% of Ag: 11.9).

of the bandgap of TiO_2, which improves the separation efficiency of photoinduced carriers.

The SPS response signals of $Ag@TiO_2$ nanoparticles in Figure 4 (see B and C) are much weaker than those of TiO_2 nanoparticles in Figure 4 (see A) at the same calcination temperature, and the red shift of SPS response peaks of $Ag@TiO_2$ nanoparticles in Figure 4 (see C) is much clearer than that of TiO_2 nanoparticles in Figure 4 (see A), both of which are attributed to the effective trapping of photoinduced electrons by the Ag core. Additionally, no SPS signal of a mixture appeared in the SPS spectra when we mixed the same amount of Ag nanoparticles with TiO_2 nanoparticles prepared in the same system of inverse emulsion, because the amount of free Ag nanoparticles was too great.[22,25,26] All these results reveal that Ag nanoparticles were effectively coated with TiO_2 and the presence of the Ag core had an inarguable effect on the SPS signals. On the basis of the SPS responses of $Ag@TiO_2$ nanoparticles with 10.2 and 11.9 wt.-% of Ag, in Figure 4 (see B and C), it is concluded that the SPS response of $Ag@TiO_2$ nanoparticles becomes weaker with an increase in the amount of Ag, because this implies a decrease in the amount of TiO_2 on the surface of the Ag core. In fact, when the wt.-% of Ag in $Ag@TiO_2$ nanoparticles is more than 35.7%, there is no SPS response of $Ag@TiO_2$ nanoparticles at any calcination temperature.

The SPS response signals of $Ag@TiO_2$ and TiO_2 nanoparticles should become stronger with increasing calcination temperature if the size of the nanoparticles had been the only factor influencing SPS response. However, the SPS signals in the range of 500–700 °C for both $Ag@TiO_2$ and TiO_2 nanoparticles in Figure 4 weaken with increasing calcination temperature, which can obviously be attributed to the change of the surface properties of the nanoparticles in this temperature range. TG-DTA and FTIR spectra indicate that the dissociation of hydroxyl groups from the shell surface of $Ag@TiO_2$ nanoparticles takes place in the range of 500–700 °C. The surface hydroxyl groups can play an important role in the photocatalytic actions because the photoinduced holes can attack the surface hydroxyl group and yield a surface-bound OH radical, which efficiently hinders the recombination of electrons and holes.[27] The results of the SPS investigation are in good accordance with those of the TG-DTA and FTIR spectra.

The $Ag@TiO_2$ nanoparticles prepared in w/o emulsions are expected to have a higher photocatalytic activity on the basis of their special SPS responses according to an intrinsic relationship between the SPS response and the photocatalytic activity of TiO_2 or ZnO nanoparticles, i.e. the weaker the SPS signal, the higher the photocatalytic activity.[22] The photocatalytic activity of the $Ag@TiO_2$ nanoparticles is under study.

Conclusions

In summary, we have demonstrated that $Ag@TiO_2$ core-shell nanoparticles could be prepared in water-in-oil emulsions. Such a novel method should be adapted to the preparation of other core-shell metal nanoparticles with oxide shells. The SPS results indicate that $Ag@TiO_2$ nanoparticles

 © 2005 Wiley-VCH Verlag GmbH & Co. KGaA, Weinheim

Table 1. SPS data of TiO_2 and Ag@TiO_2 particles calcined at various temperatures.

Sample[a]	Ag component [wt.-%]	Calcination temperature [°C]	Particle size[b] [nm]	Threshold [eV]	SPV [μV]
A	0	500	45.81	3.05	126.87
A	0	600	52.63	3.01	18.77
A	0	700	68.66	2.99	5.79
A	0	800	115.09	2.92	180.27
B	10.2	500	50.19	3.12	48.25
B	10.2	600	62.45	3.06	16.43
B	10.2	700	70.18	3.02	4.83
B	10.2	800	180.12	2.96	85.28
C	11.9	500	53.42	3.19	15.13
C	11.9	600	66.35	3.10	2.84
C	11.9	700	73.47	3.05	2.37
C	11.9	800	185.31	2.98	18.56

[a] Sample A is TiO_2 nanoparticles. Samples B and C are Ag@TiO_2 nanoparticles corresponding to 10.2 and 11.9 wt.-% of Ag. [b] Obtained from the XRD data by the Scherrer equation: $D = k\lambda/\beta\cos\theta$.

prepared in water-in-oil emulsions have potential applications in photoinduced electron storage and photocatalysis.

Experimental Section

Transmission electron microscopy (TEM) measurements were performed with a Hitachi H-8100 transmission electron microscope. The samples were prepared on carbon-coated copper grids. X-ray diffraction studies were carried out with a Rigaku wide-angle X-ray diffractometer (D/max γA using Cu-K_α radiation at λ = 1.541 Å). The detector was calibrated by using KCl powder as a standard [2θ = 28.345° (200) and 40.507° (220) under Cu-K_α radiation]. IR spectroscopic measurements were performed with a Nicolet Avatar 360 FTIR spectrometer. Surface photovoltaic spectroscopy (SPS) studies were carried out with a home-built apparatus which had a solid junction photovoltaic cell (ITO/sample/ITO) using the light source-monochromator lock-in detection technique. The measurements were performed at room temperature. Thermal analyses (TG-DTA) were carried out with a Rigaku DTG60H thermal analyzer working at a heating rate of 20 °C /min, with α-Al_2O_3 as the reference material.

Two nonionic surfactants, Span80 and Op10, were used for the preparation of w/o emulsions in this work. In a typical preparation procedure of Ag@TiO_2 nanoparticles, in order to obtain an inverse emulsion containing Ag nanoparticles, the water phase [8 mL of 2% (m/v) Tollens reagent (containing 0.59 mmol Ag^+) and 2 mL of an aqueous 10% (m/v) glucose solution] was added to the oil phase (70 mL of toluene containing 13.9 mmol of Span80 and 1.5 mmol of Op10). The mixture was stirred vigorously under nitrogen for 1 h at room temperature. Further stirring with a moderate agitation intensity at 60 °C for 3 h resulted in a brown-black dispersion, which indicated the formation of Ag-nanoparticle colloids. The coating of TiO_2 was carried out as follows: equimolar (5.9 mmol) amounts of $Ti(OC_4H_9)_4$ (TOB) and acetylacetone were mixed under sonication in a standard ultrasound bath for a few minutes and then added to the above dispersion. Acetylacetone was used as a chelating agent to control the hydrolysis and condensation of TOB.[4] The mixture was stirred under nitrogen at 60 °C for 9 h to give a solution containing Ag@TiO_2 nanoparticles, which was used for TEM measurements. The solution was vacuum dried at 60 °C for 72 h to give a viscous residue, which was analyzed by TG-DTA. The viscous residue was calcined at 300–800 °C for 4 h and then characterized by IR, XRD, and SPS measurements.

Acknowledgments

The work was supported by the National Natural Science Foundation of China (20274014).

[1] R. T. Tom, A. S. Nair, N. Singh, M. Aslam, C. L. Nagendra, R. Philip, K. Vijayamohanan, T. Pradeep, *Langmuir* **2003**, *19*, 3439–3445.
[2] A. Ueno, N. Kakuta, K. H. Park, M. F. Finlayson, A. J. Bard, A. Campion, M. A. Fox, S. E. Webber, J. M. White, *J. Phys. Chem.* **1985**, *89*, 3828–3833.
[3] C. Nasr, H. S. Chandini, W. Y. Kim, R. H. Schmehl, P. V. Kamat, *J. Phys. Chem. B* **1997**, *101*, 7480–7487.
[4] I. Pastoriza-Santos, D. S. Koktysh, A. A. Mamedov, M. Giersig, N. A. Kotov, L. M. Liz-Marzan, *Langmuir* **2000**, *16*, 2731–2735.
[5] K. Kalyanasundaram, M. Gratzel, *Optoelectronic Properties of Inorganic Solids* (Eds.: D. M. Roundhill, J. P. Fackler), Plenum Press, New York, **1999**, p. 169.
[6] I. Pastoriza-Santos, L. M. Liz-Marzan, *Langmuir* **1999**, *15*, 948–951.
[7] T. Ung, L. M. Liz-Marzan, P. Mulvaney, *J. Phys. Chem. B* **1999**, *103*, 6770–6773.
[8] L. M. Liz-Marzan, M. Giersig, P. Mulvaney, *Langmuir* **1996**, *12*, 4329–4335.
[9] S. Link, Z. L. Wang, M. A. El-Sayed, *J. Phys. Chem. B* **1999**, *103*, 3529–3533.
[10] L. M. Liz-Marzan, A. P. Philipse, *J. Phys. Chem.* **1995**, *99*, 15120–15128.
[11] Y. Mizukoshi, K. Okitsu, Y. Maeda, T. A. Yamamoto, R. Oshima, Y. Nagata, *J. Phys. Chem. B* **1997**, *101*, 7033–7037.
[12] M. Treguer, C. Cointet, H. Remita, J. Khatouri, M. Mostafavi, J. Amblard, J. Belloni, R. Keyzer, *J. Phys. Chem. B* **1998**, *102*, 4310–4321.
[13] G. C. Papavassiliou, *J. Phys. F: Met. Phys.* **1976**, *6*, L103.
[14] M. Boutonnet, J. Kizling, P. Stenius, G. Maire, *Colloids Surf.* **1982**, *5*, 209–217.
[15] K. Osseo-Asare, F. Arriagada, *J. Colloid Interface Sci.* **1990**, *50*, 321–327.
[16] N. Moumen, M. P. Pileni, R. A. Mackay, *Colloid Surf. A* **1999**, *151*, 409–417.
[17] L. Armelao, R. Bertoncello, E. Cattaruzza, S. Gialanella, S. Gross, G. Mattei, P. Mazzoldi, E. Tondello, *J. Mater. Chem.* **2002**, *12*, 2401–2407.
[18] L. Q. Jing, X. J. Sun, W. M. Cai, Z. L. Xu, Y. G. Du, H. G. Fu, *J. Phys. Chem. Solids* **2003**, *64*, 615–623.
[19] Z. Qinghong, G. Lian, G. Jingkun, B. McKinney, M. Rouse, *Appl. Catal. B* **2000**, *26*, 207–215.

 © 2005 Wiley-VCH Verlag GmbH & Co. KGaA, Weinheim

[20] N. Yoshio, K. Mitsuo, N. Junichi, *J. Phys. Chem. B* **1998**, *102*, 10279–10283.
[21] K. Nauka, T. I. Kamins, *J. Electrochem. Soc.* **1999**, *146*, 292–299.
[22] L. Q. Jing, X. J. Sun, J. Shang, W. M. Cai, Z. L. Xu, Y. G. Du, H. G. Fu, *Sol. Energy Mater. Sol. Cells* **2003**, *79*, 133–151.
[23] X. M. Qian, X. T. Zhang, Y. B. Bai, *J. Nanopart. Res.* **2000**, *2*, 191–198.
[24] L. Q. Jing, Z. L. Xu, *Appl. Surf. Sci.* **2001**, *180*, 308–314.
[25] M. Sadeghi, W. Liu, *J. Phys. Chem.* **1996**, *100*, 19466–19474.
[26] N. J. Renault, *J. Phys. Chem.* **1986**, *90*, 2732–2743.
[27] L. Q. Jing, Y. G. Zhang, Z. L. Xu, *J. Chin. Univ.* **2001**, *22*, 1885–1888.

Received: September 28, 2004

 © 2005 Wiley-VCH Verlag GmbH & Co. KGaA, Weinheim